

Structures and Properties of the Perovskite-Type Compounds $\text{Na}_{1-x}\text{Sr}_x\text{NbO}_3$ ($0.1 \leq x \leq 0.9$)—From Insulating to Metallic Conductivity

S. Ya. Istomin,* G. Svensson,† and J. Köhler‡¹

*Department of Chemistry, Moscow State University, 119899 Moscow, Russia; †Department of Structural Chemistry, Stockholm University, 10691 Stockholm, Sweden; and ‡Max-Planck-Institut für Festkörperforschung, Heisenbergstr. 1, D-70569 Stuttgart, Germany

Received November 15, 2001; in revised form March 28, 2002; accepted April 5, 2002

Reduced perovskite-type compounds with compositions $\text{Na}_{1-x}\text{Sr}_x\text{NbO}_3$ ($0.1 \leq x \leq 0.9$) have been synthesized. X-ray powder diffraction (XRD) studies for the $0.2 \leq x \leq 0.7$ phases indicate a tetragonal structure ($P4/mbm$) with unit-cell parameters $a \approx \sqrt{2} \times a_{\text{per}}$, $c \approx a_{\text{per}}$ (the subscript 'per' refers to the cubic perovskite structure), and for $x = 0.8$ and 0.9 , the space group $P4/mmm$ was found with $a \approx a_{\text{per}}$, $c \approx a_{\text{per}}$. Structure refinements based on XRD and neutron diffraction data using the Rietveld technique confirmed this for $\text{Na}_{1-x}\text{Sr}_x\text{NbO}_3$, $0.3 \leq x \leq 0.7$ and $x = 0.5, 0.6$, respectively. Selected-area and convergent beam electron diffraction studies show that the crystallites of $x = 0.2$ and 0.3 phases in fact have the GdFeO_3 -type structure (space group $Pnma$ and unit-cell parameters $a \approx \sqrt{2} \times a_{\text{per}}$, $b \approx 2 \times a_{\text{per}}$, $c \approx \sqrt{2} \times a_{\text{per}}$) while crystallites in the $0.4 \leq x \leq 0.9$ samples consist of intergrown domains between this orthorhombic structure and the tetragonal structure ($P4/mbm$). The reason for the appearance of two phases is due to local variations in the Na/Sr content within the crystallites. Measurements of the magnetic susceptibilities show that the itinerant behavior in the samples $\text{Na}_{1-x}\text{Sr}_x\text{NbO}_3$ increases with the carrier concentration. The resistivity measurements indicate that an insulator–metal transition takes place between $x = 0.5$ and 0.6 . The samples with $x = 0.4$ and 0.5 exhibit a complex temperature dependence of the resistivity with a maximum around 70 K. © 2002 Elsevier Science (USA)

Key Words: sodium niobate; strontium niobate; perovskite; electrical transport properties; magnetic properties.

INTRODUCTION

There are only a small number of reported studies on composition-induced metal–insulator transitions in complex perovskite-type oxides of transition metals with d^0-d^1 electronic configuration. The most obvious conditions which have to be fulfilled for such a transition to take

place are the presence of enough charge carriers and the occurrence of suitable paths of overlapping orbitals, which requires that the tilt of the NbO_6 octahedra should not be too large (1). However, the situation in reality is often much more complicated, as found for example in $\text{SrNbO}_{3.41}$ (2), $\text{A}_{1-x}\text{Re}_x\text{TiO}_3$ (3) and Nd_xTiO_3 (4).

For several years we have been interested in these types of transitions in reduced d^0-d^1 oxoniobates and oxotantalates. Recently, we reported the synthesis of the first reduced oxotantalates with perovskite-type structure $\text{Na}_{1-x}\text{Sr}_x\text{TaO}_3$ ($0.0 \leq x \leq 0.4$) (5, 6). In this system, the resistivity decreases with increasing strontium content but metallic conductivity was not reached even for the highest strontium content $\text{Na}_{0.6}\text{Sr}_{0.4}\text{TaO}_3$. The most probable reason for this is that high enough charge carrier concentrations are not achieved in the conductivity band. The structural studies of the $\text{Na}_{1-x}\text{Sr}_x\text{TaO}_3$ system ($0 < x \leq 0.4$) reveal that the introduction of strontium decreases the tilting of the TaO_6 octahedra. NaTaO_3 belongs to the three-tilt system $a^-b^+a^-$ using Glazer's notation (7) and crystallizes like the $x = 0.1$ and 0.2 compounds in the space group $Pnma$. According to ED studies, crystallites of the $x = 0.3$ and 0.4 samples are inhomogeneous and exhibit intergrowths between domains of the one-tilt system $a^0a^0c^+$ ($P4/mbm$) and the three-tilt system $a^-b^+a^-$ ($Pnma$). An additional NPD study of the $x = 0.2$ and 0.3 samples shows the former to have a three-tilt $a^-b^+a^-$ and the later a single-tilt distortion $a^0a^0c^+$ of the perovskite structure (6).

The system $\text{Na}_{1-x}\text{Sr}_x\text{NbO}_3$ ($0.0 \leq x \leq 0.6$) was investigated by Ellis *et al.* some years ago (8, 9). They observed an increasing electrical conductivity with increasing Sr content, although a metal-like temperature dependence was never obtained. It is often possible to increase the homogeneity range of solid solutions of this type by simply increasing the synthesis temperature. An increased x value should at least result in a metal–insulator transition since SrNbO_3 is metallic (10). We have synthesized the solid

¹To whom correspondence should be addressed. Fax: 0711-689-1642. E-mail: j.koehler@fkf.mpg.de.



solution $\text{Na}_{1-x}\text{Sr}_x\text{NbO}_3$ up to $x = 0.9$ and found a compositional semiconductor–metal transition between $x = 0.5$ and 0.6 . In order to obtain a detailed structural information of these compounds, especially with respect to the tilting of the NbO_6 octahedra, we have performed neutron diffraction studies.

EXPERIMENTAL

Samples of $\text{Na}_{1-x}\text{Sr}_x\text{NbO}_3$ ($0 \leq x \leq 0.9$) were prepared by annealing pellets of stoichiometric mixtures of NaNbO_3 , $\text{Sr}_5\text{Nb}_4\text{O}_{15}$ and Nb (99.99%) in niobium tubes, sealed by welding under Ar, at 1350–1400°C for 17–24 h. NaNbO_3 and $\text{Sr}_5\text{Nb}_4\text{O}_{15}$ were prepared by heating stoichiometric amounts of Na_2CO_3 and Nb_2O_5 at 1000°C for 48 h, and SrCO_3 and Nb_2O_5 at 1200°C for 48 h in air, respectively. X-ray powder diffraction (XRD) data were collected on an STOE STADI-P powder diffractometer. $\text{CuK}\alpha_1$ radiation and Si as internal standard were used in both cases. Neutron powder diffraction data of the $x = 0.5$ and 0.6 samples were collected on the NPD diffractometer at the Swedish research reactor R2 at NFL, Studsvik. A single monochromator, Cu (220), was set to give a wavelength of 1.47(1) Å. After collimating, the neutron flux at the sample position was $1 \times 10^6 \text{ n cm}^{-2} \text{ s}^{-1}$. The instrument had 38 Reuter–Stokes ^3He position-sensitive detectors. Complete angular coverage was obtained with two positions of the detector box. The instrumental half-width was 0.6° at $2\theta = 56^\circ$. The sample ($\sim 2.5 \text{ g}$) was contained in a vanadium tube (i.d. = 6 mm). The RIETAN 97 program package was used for the structural refinement (11) based on both the XRD and NPD data. Scattering amplitudes used in the NPD refinement were $0.49 \times 10^{-12} \text{ cm}$ for Sr, $0.72 \times 10^{-12} \text{ cm}$ for Na and $0.691 \times 10^{-12} \text{ cm}$ for Nb.

The magnetic susceptibilities of a sample of $\text{Na}_{1-x}\text{Sr}_x\text{NbO}_3$, $0.1 \leq x \leq 0.9$ samples were measured using an MPMS Quantum Design SQUID at an external magnetic field of 5 T as a function of temperature. The resistivities of the $\text{Na}_{1-x}\text{Sr}_x\text{NbO}_3$ ($0.1 \leq x \leq 0.9$) samples were measured on pellets approximately $3 \times 4 \times 4 \text{ mm}$ in size by a normal four-probe method in the temperature range 2–300 K.

RESULTS

After heat treatment, the $\text{Na}_{1-x}\text{Sr}_x\text{NbO}_3$ samples were blue with an increasing red luster at higher Sr contents, see Table 1. Often additional red crystallites were found at those parts of the tablets, which have been close to the Nb tube wall, and sometimes large areas of red crystallites were present, mainly at the surfaces of the tablets. This is not surprising since the color of Sr_xNbO_3 varies from blue for $x = 0.70$ to red for $x = 0.90$ (12). Monophasic samples of $\text{Na}_{1-x}\text{Sr}_x\text{NbO}_3$, $0.3 \leq x \leq 0.9$, were prepared at 1400°C. At this temperature, the $x = 0.1$ and 0.2 samples had partially melted into the niobium tube. An $x = 0.2$ sample was, therefore, synthesized a second time at 1350°C.

The cation contents of the samples, as obtained from the SEM–EDS analysis, are given in Table 2. They indicate the Na/Sr ratios to be close to nominal, and all samples to be Sr/Na deficient under the assumption of fully occupied niobium positions. The chemical formula may therefore be written as $(\text{Na}_{1-x}\text{Sr}_x)_{1-y}\text{NbO}_3$ ($0.0 \leq x \leq 1.0$ and $y \approx 0.1$). The presence of vacancies at the A-position in ABO_3 is not surprising, since Sr_xNbO_3 has a wide homogeneity range: $0.75 \leq x \leq 0.95$ (12), and sodium is quite volatile at the syntheses temperatures used. SEM–EDS and TEM–EDS of red crystallites found in a sample with $x = 0.5$ heated once at 1400°C showed that they have a higher Sr content

TABLE 1
Color, Crystal Data for $\text{Na}_{1-x}\text{Sr}_x\text{NbO}_3$, $0.2 \leq x \leq 0.9$ as Obtained from the XRD Studies, and Selected Details from the Corresponding Structural Refinements

| x | 0.2 ^{a,b} | 0.3 ^c | 0.4 ^c | 0.5 ^c | 0.6 ^c | 0.7 ^c | 0.8 ^c | 0.9 ^a |
|-----------------------------|--------------------|----------------------|----------------------|----------------------|----------------------|----------------------|------------------|------------------|
| Color | Dark gray | Light blue | Blue | Blue | Blue-violet | Blue-violet | Dark red | Red |
| Unit-cell axis; | 5.5721(8) | 5.58107(7) | 5.60007(7) | 5.61855(7) | 5.63592(7) | 5.65824(9) | 4.0025(3) | 4.0192(5) |
| a, c (Å) | 3.9275(7) | 3.96585(6) | 3.97721(5) | 3.98714(5) | 3.99604(5) | 3.99270(8) | 4.0080(3) | |
| Space group | $P4/mbm$ | $P4/mbm$ | $P4/mbm$ | $P4/mbm$ | $P4/mbm$ | $P4/mbm$ | $P4/mmm$ | $Pm3m$ |
| Z | 2 | 2 | 2 | 2 | 2 | 2 | 2 | 1 |
| Cell vol. (Å ³) | 121.9 (61.0) | 123.5 (61.8) | 124.7 (62.4) | 126.0 (63.0) | 126.9 (63.5) | 127.8 (63.9) | 64.2 | 64.9 |
| 2θ -range (deg) | | $15 < 2\theta < 110$ | | |
| Step length, 2θ | | 0.01 | 0.01 | 0.01 | 0.01 | 0.01 | | |
| R_I, R | | 0.019, 0.039 | 0.032, 0.054 | 0.019, 0.044 | 0.029, 0.060 | 0.014, 0.052 | | |
| S | | 1.58 | 1.20 | 1.31 | 1.15 | 1.09 | | |

^a Guinier techniques.

^b Prepared at 1350°C.

^c X-ray powder diffractometer.

TABLE 2
EDX Analysis Data for $\text{Na}_{1-x}\text{Sr}_x\text{NbO}_3$, $0.3 \leq x \leq 0.9$

| Initial composition | Calculated cation ratio Na:Sr:Nb (at%) | EDX analysis data Na:Sr:Nb (at%) |
|--|---|-------------------------------------|
| $\text{Na}_{0.7}\text{Sr}_{0.3}\text{NbO}_3$ | 35:15:50 | 30(2):16(3):54(1) |
| $\text{Na}_{0.6}\text{Sr}_{0.4}\text{NbO}_3$ | 30:20:50 | 28(2):19(1):53(1) |
| $\text{Na}_{0.5}\text{Sr}_{0.5}\text{NbO}_3$ | 25:25:50 | 22(2):24(1):54(1) |
| $\text{Na}_{0.4}\text{Sr}_{0.6}\text{NbO}_3$ | 20:30:50 | 19(2):27(1):54(1) |
| $\text{Na}_{0.3}\text{Sr}_{0.7}\text{NbO}_3$ | 15:35:50 | 15(2):32(1):52(1) |
| $\text{Na}_{0.2}\text{Sr}_{0.8}\text{NbO}_3$ | 10:40:50 | 10(2):37(1):53(2) |
| $\text{Na}_{0.1}\text{Sr}_{0.9}\text{NbO}_3$ | 5:45:50 | 4(2):42(2):54(1) |

than the surrounding blue crystallites. Most of the red crystallites disappeared after repeatedly grinding and annealing, although a red surface together with areas of metallic niobium was present at areas close to the tube wall. These red crystallites contained very low amounts of sodium, in some cases too low to be detected by EDS.

The resistivities of the samples $\text{Na}_{1-x}\text{Sr}_x\text{NbO}_3$, ($0.1 \leq x \leq 0.9$) range over 8 orders of magnitude from 10^{-4} to $10^4 \Omega \text{cm}$, see Fig. 1. The samples with low carrier concentrations ($x = 0.1-0.3$) are insulating and the resistivities increase with decreasing temperature. An interesting behavior is found for the $x = 0.4$ and 0.5 samples, which might be semiconducting and exhibit non-monotonic temperature behavior. Their resistivities increase with temperatures up to a maximum between $T = 70$ and 80 K . Samples with higher carrier concentrations, $0.6 \leq x \leq 0.9$, show a temperature dependency of the resistivity as typically found in metals. A change from semiconducting to metal-like behavior has taken place between $x = 0.5$ and 0.6 .

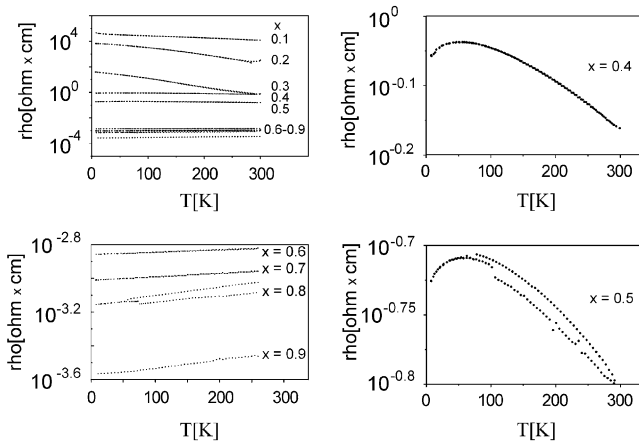


FIG. 1. Resistivity vs temperature for $\text{Na}_{1-x}\text{Sr}_x\text{NbO}_3$ ($0.1 \leq x \leq 0.9$) together with the corresponding curves for the $x = 0.4, 0.5$ and $0.6-0.9$ samples with an enlarged scale.

The magnetic susceptibilities of the $\text{Na}_{1-x}\text{Sr}_x\text{NbO}_3$, $0.1 \leq x \leq 0.9$ samples, which have not been corrected for diamagnetic contribution, show that they are all paramagnetic, see Fig. 2a. Furthermore, it can be seen that the paramagnetic susceptibilities increase with the carrier concentration, see Fig. 2b. It is remarkable that for the samples with small carrier concentration ($x = 0.1$ and 0.2) discontinuities of the temperature dependence of χ -mol are observed at approximately 160 and 60 K , respectively, see Fig. 2c. However, this change of χ -mol is so small that it is probably more related to a structural change rather than to a change in the magnetic structure.

The XRD patterns of the $\text{Na}_{1-x}\text{Sr}_x\text{NbO}_3$, $0.2 \leq x \leq 0.8$ samples, all exhibited distinct splitting of the perovskite subcell reflections, which suggest tetragonal unit cells with $a \approx a_{\text{per}}$, and $c \approx a_{\text{per}}$. This is in agreement with what has been reported by Ellis *et al.* (8, 9) for $\text{Na}_{1-x}\text{Sr}_x\text{NbO}_3$, $0.15 \leq x \leq 0.60$. However, in contrast to their results, we observed additional reflections for the $0.2 \leq x \leq 0.7$ samples, which could all be accounted for by a larger unit cell: $a \approx \sqrt{2} \times a_{\text{per}}$, $c \approx a_{\text{per}}$. Reflections of the type $h00 \rightarrow h = 2n+1$ were systematically absent, indicating the space group to be $P4/mbm$. This corresponds to the single $a^0 a^0 c^+$ tilt system according to Glazer. No superstructure reflections could be found in the XRD patterns of the $x = 0.8$ and 0.9 samples. The XRD pattern for $x = 0.9$ sample showed no clear splitting, although a plot of full-width at half-maximum (FWHM) vs 2Θ revealed that the cell, in fact, is not cubic, as shown in Fig. 3. The splitting of the reflections was very small and only a cubic unit cell $a = 4.0192(5) \text{ \AA}$ could be refined. The unit-cell parameters from the XRD study are given in Table 2. The volume of the perovskite subcell in $\text{Na}_{1-x}\text{Sr}_x\text{NbO}_3$, $0.2 \leq x \leq 0.9$ increases with the Sr content (x), as shown in Fig. 4.

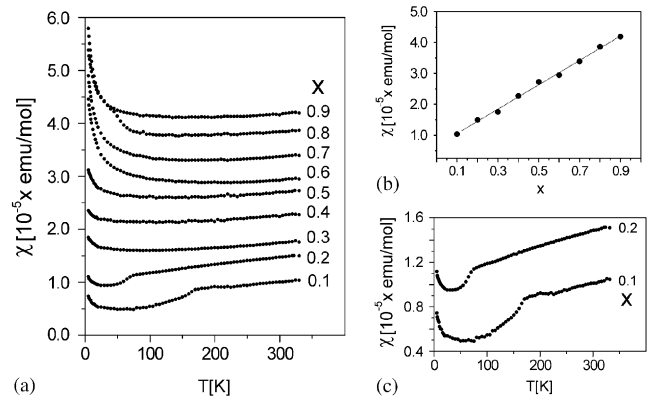


FIG. 2. (a) Temperature dependence of the magnetic susceptibilities (without diamagnetic correction) at an external magnetic field of 5 T vs temperature for samples $\text{Na}_{1-x}\text{Sr}_x\text{NbO}_3$ ($0.1 \leq x \leq 0.9$) and (b) magnetic susceptibilities of samples $\text{Na}_{1-x}\text{Sr}_x\text{NbO}_3$ ($0.1 \leq x \leq 0.9$) at room temperature as a function of x and (c) magnetic susceptibilities vs temperature for $\text{Na}_{0.9}\text{Sr}_{0.1}\text{NbO}_3$ and $\text{Na}_{0.8}\text{Sr}_{0.2}\text{NbO}_3$.

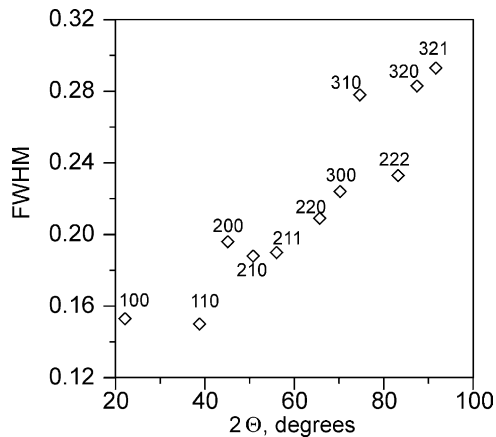


FIG. 3. Tetragonal symmetry is indicated by the non-monotonic increase of full-width at half-maximum (FWHM) of the XRD reflections with increasing Bragg angle (2θ) in the sample with the nominal composition $\text{Na}_{0.1}\text{Sr}_{0.9}\text{NbO}_3$.

This increase in volume is a combined effect of the substitution of the larger cation radius of Sr^{2+} ($r(\text{Sr}^{2+}) = 1.44 \text{ \AA}$) for Na^+ ($r(\text{Na}^+) = 1.39 \text{ \AA}$) and the increase of the ionic radius of Nb cation due to the partial reduction of Nb^{5+} ($r(\text{Nb}^{5+}) = 0.64 \text{ \AA}$) to Nb^{4+} ($r(\text{Nb}^{4+}) = 0.68 \text{ \AA}$) (13).

ELECTRON DIFFRACTION

Selected-area electron diffraction (SAED) and convergent beam electron diffraction (CBED) studies were performed on all $\text{Na}_{1-x}\text{Sr}_x\text{NbO}_3$ samples. Typically, the $hk0_{\text{per}}$ and hhl_{per} patterns were recorded and in addition patterns with the beam aligned along $\langle 310 \rangle_{\text{per}}^*$ (asterisk indicates reciprocal space) which lies between these first orientations when tilting. Two such series of patterns recorded from one crystal in the $x = 0.3$ and one in the 0.8 sample are shown in Figs. 5 and 6. In many cases, the corresponding CBED patterns viewed along $\langle 001 \rangle_{\text{per}}$

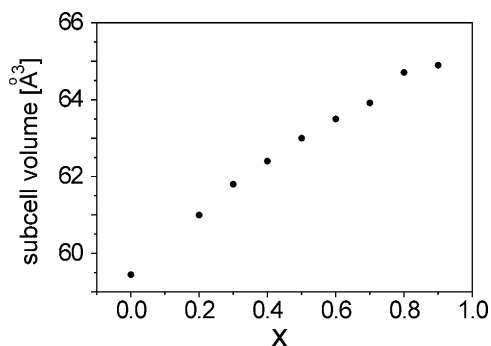


FIG. 4. The volume of the perovskite subcell (a_{per}^3) of $\text{Na}_{1-x}\text{Sr}_x\text{NbO}_3$ vs x .

were recorded as well. Two such patterns of the same crystallites as those in Figs. 5 and 6 are shown in Figs. 7 and 8, respectively. Fourfold symmetry was never observed in the CBED patterns of crystallites of the $x = 0.2$ and 0.3 samples, while it often was observed in the $0.4 \leq x \leq 0.8$ samples, e.g. Figs. 7 and 8. However, it has to be mentioned that the fourfold symmetry was only found in limited areas and disappeared when the beam or crystal was moved only a bit. The $hk0_{\text{per}}$ SAED patterns were always consistent with the unit-cell parameters, $a \approx b \approx \sqrt{2} \times a_{\text{per}}$ and $c \approx a_{\text{per}}$, obtained in the XRD study and the general trend was that the intensities of the superstructure reflections decreased with increasing Sr content. Reflections indicating a doubling of any perovskite axis were never observed in the $hk0_{\text{per}}$ patterns. The SAED patterns recorded along $\langle 310 \rangle_{\text{per}}^*$ very often exhibited streaking along $\langle 001 \rangle_{\text{per}}^*$ for the $hk1/2l$ set of reflections indicating disorder, as shown in Figs. 5 and 6. This streaking very often had intensity maximum at $k = \frac{1}{2} \langle 001 \rangle_{\text{per}}^*$ which can only be accounted for with a doubling of at least one of the perovskite subaxis, e.g. $a \approx b \approx \sqrt{2} \times a_{\text{per}}$ and $c \approx 2 \times a_{\text{per}}$. This supercell was also supported by superstructure reflections at $k = \frac{1}{2} \langle 111 \rangle_{\text{per}}^*$ in the hhl_{per} patterns of most crystallites in all samples, see e.g. Figs. 5 and 6. The intensities of these superstructure reflections varied within the crystallites and were weaker and disappeared locally when the overall Sr content of the sample was high, $x \geq 0.5$. It should be mentioned that superstructure reflections of the kind $hh1/2l_{\text{per}}$ were never observed in the hhl_{per} patterns. A merging of the results from the XRD and SAED studies of the $0.4 \leq x \leq 0.8$ samples, therefore, propose that the unit cells are tetragonal with $a = b \approx \sqrt{2} \times a_{\text{per}}$ and $c \approx 2 \times a_{\text{per}}$. The reflection conditions $h00, 0k0 \rightarrow h, k = 2n$ found in the XRD study were confirmed by the presence of Gjønnes–Moodie lines in most of the CBED patterns viewed along $\langle 001 \rangle_{\text{per}}$, see e.g. in Figs. 7 and 8. Furthermore, a study of the SAED patterns shows that the reflection conditions $0kl \rightarrow k + l = 2n, hhl \rightarrow l = 2n, 00l \rightarrow l = 2n$ and $00k \rightarrow k = 2n$ are always valid for both orthorhombic unit cells for the $x = 0.2$ and 0.3 compounds and the tetragonal ones for the $0.4 \leq x \leq 0.8$ compounds. A rigid interpretation of these results, therefore, leads to the space group $Pnma$ for the $x = 0.2$ and 0.3 compounds, while the observation of fourfold symmetry in the $0.4 \leq x \leq 0.8$ compounds leads to the space group $P4/mnc$ and $P4nc$. These space groups are not frequently found among perovskites, although elpasolites sometimes crystallize in one of them (14). More important are the superstructures with these space groups, which are not accessible by a tilting of regular NbO_6 octahedra (7), as it is shown by structure refinements discussed below. However, as mentioned above, streaking indicating disorder was frequently (nearly always) observed in the SAED patterns recorded along $\langle 310 \rangle_{\text{per}}^*$. The

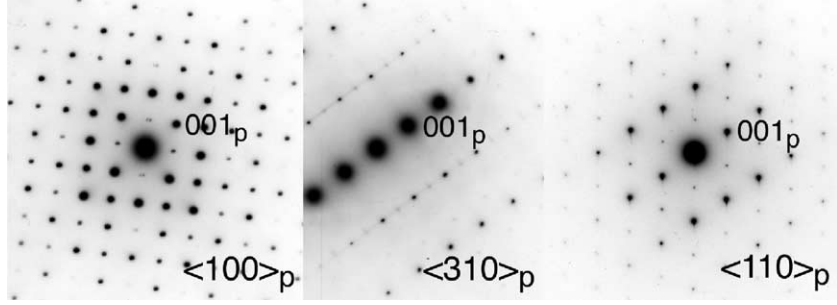


FIG. 5. SAED patterns of crystallites found in $\text{Na}_{1-x}\text{Sr}_x\text{NbO}_3$, $x = 0.3$. Left: An $hk0$ ED pattern, zone axis $[010]_{Pnma} = \langle 001 \rangle_{\text{per}}([010]_{Pnma})$ corresponds to the zone axis in space group $Pnma$ with unit-cell parameters $a \approx \sqrt{2} \times a_{\text{per}}$, $b \approx 2 \times a_{\text{per}}$ and $c \approx \sqrt{2} \times a_{\text{per}}$, and $\langle 001 \rangle_{\text{per}}$ the corresponding zone axis in ideal cubic perovskite). The reflections corresponding to $h00$ and $0k0$, $h, k \neq 2n$ are present due to multiple scattering. Center: A $0kl$ ED pattern, zone axis $[100]_{Pnma} = \langle 110 \rangle_{\text{per}}$. Reflections corresponding to $k + l \neq 2n$ are systematically absent. Right: An ED pattern viewed along the zone axis $[210]_{Pnma} = \langle 310 \rangle_{\text{per}}$. The superstructure reflections with $h + k \neq 2n$ are affected by weak streaking along the c -axis which indicates disorder.

disorder can also explain why the fourfold axis in the CBED patterns viewed along $\langle 001 \rangle_{\text{per}}$ comes and goes as the beam is moved over the crystallites. We, therefore, suggest that the crystallites in the $x \geq 0.4$ samples consist of intergrowths between domains with the single tilt ($a^0 a^0 c^+$) tetragonal structure (space group $P4/mbm$ and $a \approx \sqrt{2} \times a_{\text{per}}$, $c \approx a_{\text{per}}$) and domains having orthorhombic structure and a larger unit cell. The observed SAED patterns would then be a superimposing of these domains. There are two main orthorhombic structure candidates; the double-tilt ($a^0 b^- c^+$) with space group $Cmcm$ with $a \approx 2 \times a_{\text{per}}$, $b \approx 2 \times a_{\text{per}}$ and $c \approx 2 \times a_{\text{per}}$ and the triple-tilt ($a^- b^+ a^-$) $Pnma$ with the unit-cell parameters $a \approx \sqrt{2} \times a_{\text{per}}$, $b \approx 2 \times a_{\text{per}}$ and $c \approx \sqrt{2} \times a_{\text{per}}$. These types of distortion of the perovskite structure are frequently found among niobates and tantalates, e.g. NaNbO_3 and NaTaO_3 (15). However, the triple tilting ($a^- b^+ a^-$) with space group $Pnma$ is a stronger candidate than the double one, as it gives the same systematic reflection conditions as $P4/mnc$ and $P4nc$. In the

double-tilt structure ($a^0 b^- c^+$) with space group $Cmcm$, the reflections forbidden in the $hk0_{\text{per}} = h0l_{Pnma} = hk0_{P4/mbm}$ patterns are allowed, i.e. in the $hk0_{Cmcm}$ (subscript “ $Cmcm$ ” refers to indexing in the unit cell corresponding to $Cmcm$) pattern. The presence of GM lines in most of the CBED patterns viewed along $\langle 001 \rangle_{\text{per}}$, therefore, makes this space group less probable, although its presence in small domains cannot be excluded. A summary of the unit cells and space groups as obtained from the SAED and CBED study is given in Table 3. The results above are consistent with what has been found in the $\text{Na}_{1-x}\text{Sr}_x\text{TaO}_3$ system (5). It may, therefore, be concluded from the ED studies of $\text{Na}_{1-x}\text{Sr}_x\text{NbO}_3$ ($0.2 \leq x \leq 0.9$) that the situation is more complex than one could have expected from the XRD studies. It shows that the crystallites consist of domains with slightly different tilting of the octahedra. It varies between single ($a^0 a^0 c^+$ — $P4/mbm$ —unit-cell parameters; $a \approx \sqrt{2} \times a_{\text{per}}$, $c \approx a_{\text{per}}$), double ($a^0 b^- c^+$ — $Cmcm$; $a \approx 2 \times a_{\text{per}}$, $b \approx 2 \times b_{\text{per}}$, $c \approx 2 \times a_{\text{per}}$) and triple ($a^- b^+ a^-$ — $Pnma$;

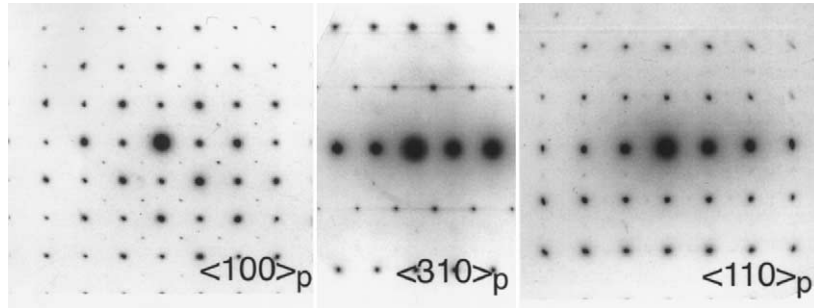


FIG. 6. SAED patterns of crystallites found in $\text{Na}_{1-x}\text{Sr}_x\text{NbO}_3$, $x = 0.8$. Left: An $hk0$ ED pattern, zone axis $[010]_{Pnma} = \langle 001 \rangle_{\text{per}}([010]_{Pnma})$ corresponds to the zone axis in space group $Pnma$ with unit-cell parameters $a \approx \sqrt{2} \times a_{\text{per}}$, $b \approx 2 \times a_{\text{per}}$ and $c \approx \sqrt{2} \times a_{\text{per}}$, and $\langle 001 \rangle_{\text{per}}$ is the corresponding zone axis in ideal cubic perovskite). The reflections corresponding to $h00$ and $0k0$, $h, k \neq 2n$ are present due to multiple scattering. Center: A $0kl$ ED pattern, zone axis $[100]_{Pnma} = \langle 110 \rangle_{\text{per}}$. Reflections corresponding to $k + l \neq 2n$ are systematically absent. Right: An ED pattern viewed along the zone axis $[210]_{Pnma} = \langle 310 \rangle_{\text{per}}$. The superstructure reflections with $h + k \neq 2n$ are affected by weak streaking along the c -axis which indicates disorder.

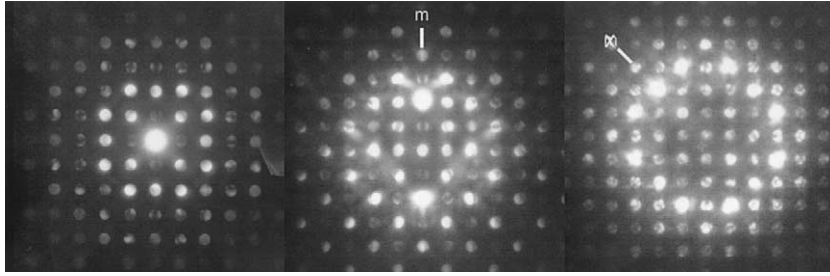


FIG. 7. CBED patterns with $2mm$ symmetry found in a crystallite in a sample with nominal composition $\text{Na}_{1-x}\text{Sr}_x\text{NbO}_3$, $x = 0.3$, viewed along $\langle 001 \rangle_{\text{per}}$. In b the crystal is tilted around $\langle 110 \rangle_{\text{per}}$ to show the mirror plane and in c around $\langle 100 \rangle$ to show the absence of a mirror plane.

$a \approx \sqrt{2} \times a_{\text{per}}$, $b \approx 2 \times b_{\text{per}}$, $c \approx \sqrt{2} \times c_{\text{per}}$) tilt systems within the same crystallite.

STRUCTURAL REFINEMENTS

The crystal structures of the $\text{Na}_{1-x}\text{Sr}_x\text{NbO}_3$, $0.2 \leq x \leq 0.7$ samples were refined using the XRD data. Irrespective of the result from the ED studies discussed above, it was decided to perform the refinement in space group $P4/mbm$ and unit-cell parameters suggested by the XRD data in

Table 2. The atomic coordinates of a high-temperature form of NaTaO_3 ($T = 893 \text{ K}$) (16) were used as a starting model. Crystal data and selected details from the refinements are given in Table 2. Atomic coordinates and isotropic temperature factors are given in Table 4. Observed, calculated and difference XRD profiles for $\text{Na}_{1-x}\text{Sr}_x\text{NbO}_3$ $x = 0.3$ and 0.7 are shown in Fig. 9a and b, respectively.

As mentioned above, in the system $\text{Na}_{1-x}\text{Sr}_x\text{NbO}_3$ a composition-induced semiconductor–metal transition takes

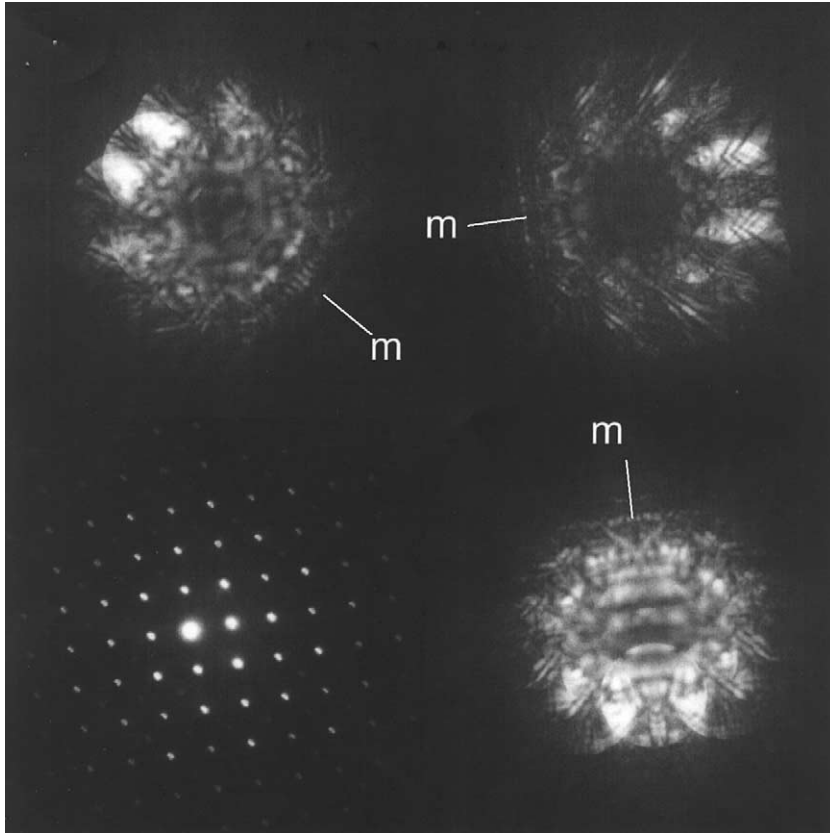


FIG. 8. CBED patterns with $4mm$ symmetry found in a crystallite in a sample with nominal composition $\text{Na}_{1-x}\text{Sr}_x\text{NbO}_3$, $x = 0.3$, viewed along $[001]_{P4/mbm} = \langle 001 \rangle_{\text{per}}$. Three CBED patterns of the same crystallite after tilting around $[100]_{P4/mbm} = \langle 110 \rangle_{\text{per}}$ and $[110]_{P4/mbm} \langle 100 \rangle$ are inserted to show the mirror planes being present due to the tetragonal symmetry.

TABLE 3
Crystal Data $\text{Na}_{1-x}\text{Sr}_x\text{NbO}_3$, $0.2 \leq x \leq 0.9$ According to the SAED and CBED Studies^a

| x | 0.2–0.3 | 0.4–0.8 | 0.9 |
|----------------|-----------------------|--|----------------------------|
| Space group | $Pnma$ | $P4/mbm$, ($Pnma$) | $Pm3m$ ($Pnma$) |
| $a/\text{\AA}$ | $\sqrt{2} \times a_p$ | $\sqrt{2} \times a_p(\sqrt{2} \times a_p)$ | $a_p(\sqrt{2} \times a_p)$ |
| $b/\text{\AA}$ | $2 \times a_p$ | $\sqrt{2} \times a_p(2 \times a_p)$ | $a_p(2 \times a_p)$ |
| $c/\text{\AA}$ | $\sqrt{2} \times a_p$ | $c_p(\sqrt{2} \times a_p)$ | $a_p(\sqrt{2} \times a_p)$ |

^aIn all samples $0.4 \leq x \leq 0.9$ CBED patterns with fourfold symmetry was observed in agreement with space groups $P4/mbm$ and $Pm3m$. However, the superstructure reflections combined with structural considerations strongly indicate the existence of domains with a larger supercell and orthorhombic symmetry ($Pnma$).

place between $x = 0.5$ and 0.6 . It was therefore decided to perform a more detailed structural study of samples having these compositions using neutron powder diffraction data. NPD data were collected from three samples one with $x = 0.5$ and two with $x = 0.6$. All reflections in the NPD patterns of the $x = 0.5$ and one of the $x = 0.6$ samples could be indexed with the tetragonal unit cell found in the XRD study. No reflections indicating a doubling of any perovskite subaxis were found, in contrast to the indications from the SAED study. Details from the structural refinements, atomic coordinates and anisotropic temperature factors are given in Tables 5, 6 and 7, respectively. The atomic coordinates are close to those obtained in the XRD study above, see Table 5. Observed, calculated and difference XRD profiles for $\text{Na}_{1-x}\text{Sr}_x\text{NbO}_3$, $x = 0.5$ are shown in Fig. 10. However, the NPD pattern of the second $x = 0.6$ sample exhibited three additional weak reflections ($2\theta = 35.540^\circ$, $I \approx 1.5\%$; $2\theta = 47.270^\circ$, $I \approx 0.5\%$ and $2\theta = 65.966^\circ$, $I \approx 1\%$), which could not be indexed with the unit cell $a \approx b \approx \sqrt{2} \times a_{\text{per}}$, $c \approx a_{\text{per}}$. These reflections could successfully be indexed on the basis of the unit cells $a \approx b \approx \sqrt{2} \times a_{\text{per}}$, $c \approx 2 \times a_{\text{per}}$ and $a \approx b \approx c \approx 2 \times a_{\text{per}}$ found

TABLE 4

Crystal Data and Selected Details from Structural Refinements of $\text{Na}_{1-x}\text{Sr}_x\text{NbO}_3$, $x = 0.5$ and 0.6 Based on Neutron Powder Diffraction Data

| x | 0.5 | 0.6 |
|-----------------------------|---------------------------|---------------------------|
| Space group | $P4/mbm$ | $P4/mbm$ |
| Unit-cell axis: | 5.6201(3) | 5.6377(3) |
| a, c (\AA) | 3.9880(3) | 3.9987(3) |
| Z | 2 | 2 |
| Cell vol (\AA^3) | 125.96 | 127.09 |
| 2θ -range (deg) | $4.00 < 2\theta < 139.92$ | $4.00 < 2\theta < 139.92$ |
| Step length, 2θ | 0.08 | 0.08 |
| R_1, R_p | 0.010, 0.0406 | 0.0071, 0.0320 |
| S | 1.22 | 1.30 |

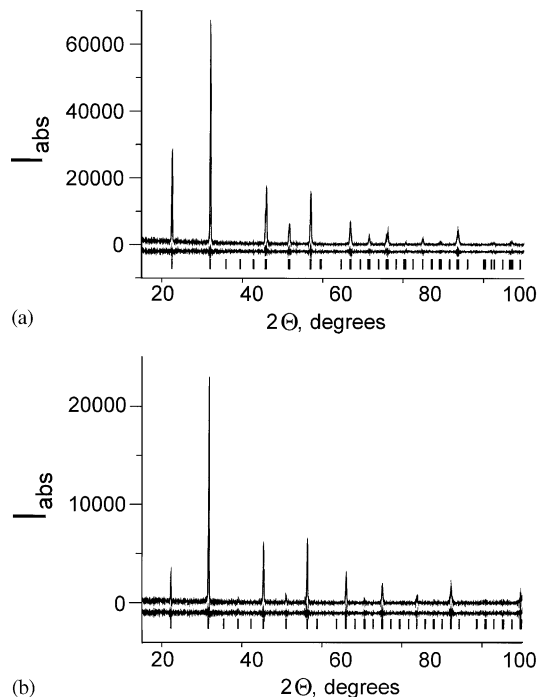


FIG. 9. Observed, calculated and difference X-ray powder-diffraction intensities of $\text{Na}_{1-x}\text{Sr}_x\text{NbO}_3$: (a) $x = 0.3$ and (b) $x = 0.7$.

in the SAED study. However, the instrumental resolution in 2θ is too low to resolve a small size difference between the a - and b -axis. A number of structure models in tetragonal as well as orthorhombic space groups with these unit-cell parameters were tested. The best results were obtained for the structure models in $Cmcm$, $a \approx 2 \times a_{\text{per}}$, $b \approx 2 \times a_{\text{per}}$, $c \approx 2 \times a_{\text{per}}$ and $Pnma$, $a \approx \sqrt{2} \times a_{\text{per}}$, $b \approx 2 \times a_{\text{per}}$, $c \approx \sqrt{2} \times a_{\text{per}}$ as found for NaNbO_3 too (15). The main

TABLE 5

Atomic Coordinates for O2, Temperature Factors (B) and Na/Sr Occupancy (g_{Na}) for $\text{Na}_{1-x}\text{Sr}_x\text{NbO}_3$, $0.3 \leq x \leq 0.9$ According to the Structure Refinements Based on the XRD Data^a

| | x | 0.3 | 0.4 | 0.5 | 0.6 | 0.7 |
|-------|------------------------|-----------|-----------|-----------|-----------|-----------|
| Na/Sr | g_{Na} | 0.71(1) | 0.66(1) | 0.53(1) | 0.44(1) | 0.3(1) |
| | B (\AA^2) | 1.24(1) | 1.15(1) | 1.16(3) | 1.06(2) | 0.87(1) |
| Nb | B (\AA^2) | 0.80(1) | 1.19(1) | 0.73(1) | 0.94(1) | 0.43(1) |
| | B (\AA^2) | 1.5(1) | 0.4(1) | 0.6(1) | 0.4(2) | 1.2(3) |
| O2 | B (\AA^2) | 1.02(6) | 0.74(7) | 0.73(7) | 0.8(1) | 0.9(1) |
| | x | 0.2794(3) | 0.2737(4) | 0.2724(4) | 0.2688(6) | 0.2686(6) |

Note. g —refined Na occupancy at the Na/Sr position.

^aThe space group is $P4/mbm$ and the atomic positions are: Na/Sr-2c, Nb-2a, O1-2b, O2-4g.

TABLE 6
Atomic Coordinates for O2, Temperature Factors (B_{eq}), and Na/Sr Occupancy (g_{Na}) for $\text{Na}_{1-x}\text{Sr}_x\text{NbO}_3$, $x = 0.5$, According to the Structure Refinements Based on the NPD Data^a

| | | x | 0.5 | 0.6 |
|-------|------------------------|-----|-----------|-----------|
| Na/Sr | $g_{\text{Na/Sr}}$ | | 0.977(5) | 0.979(5) |
| | B (\AA^2) | | 0.96 | 0.91 |
| Nb | B (\AA^2) | | 0.31 | 0.25 |
| O1 | B (\AA^2) | | 1.28 | 1.10 |
| O2 | B (\AA^2) | | 1.08 | 0.95 |
| | x | | 0.2733(3) | 0.2711(3) |

^aThe space group is $P4/mbm$ and the atomic positions are: Na/Sr-2c, Nb-2a, O1-2b, O2-4g.

difference between the calculated powder diffraction patterns is the presence of two weak reflections 112 and 332 in $Cmcm$, which are not observed on the neutron pattern. The structures are examples of double ($a^0b^-c^+$) and triple ($a^-b^+a^-$) tilting of the perovskite structure using Glazer's classification. These orthorhombic structures are the same as those discussed in the ED study above. It should be mentioned that the structure models in the tetragonal space groups $P4/mnc$ and $P4nc$ discussed above gave negative temperature factors for the cations and large ones for the oxygen atoms ($3\text{--}5\text{\AA}^2$). This supports the conclusion that these space groups are less probable.

The NPD studies confirm once more the results of the ED studies indicating that the crystallites of $\text{Na}_{1-x}\text{Sr}_x\text{NbO}_3$ samples consist of domains with slightly tilted octahedra. This is probably caused by small variations in the sodium content and vacancies concentration at the A-position. The relative amount of the different structures depends on the sample homogenization, micro-strain, temperature of the annealing, closeness of the crystallite to the surface or the pellet, etc.

DISCUSSION

Selected interatomic distances and bond angles from the structural refinements based on the XRD and NPD data

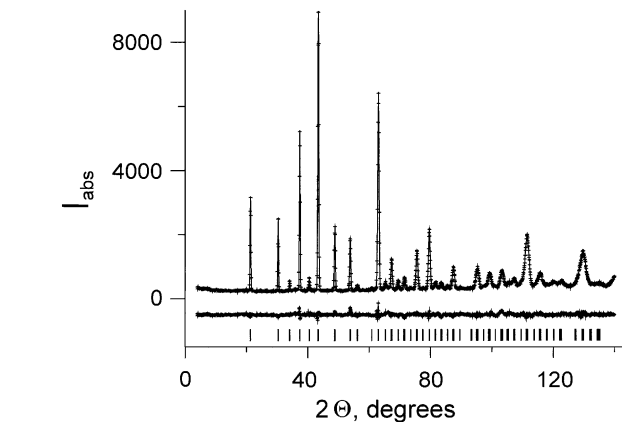


FIG. 10. Observed, calculated and difference neutron powder-diffraction intensities of $\text{Na}_{1-x}\text{Sr}_x\text{NbO}_3$, $x = 0.5$.

are given in Tables 8 and 9, respectively. The NbO_6 octahedra obtained in all the refinements (XRD and NPD data sets) are rather regular. This shows that the tilting scheme introduced by Glazer several years ago to describe distortions of the perovskite structure is applicable. The size of the NbO_6 octahedra as well as the Nb–O–Nb bond angles increases as the number of valence electrons on the Nb cation increases and the Nb–O π -bonding orbitals become occupied. Consequently, the distortion from ideal cubic structure decreases with increasing Sr content (x value). These changes also influence the size and distortion of the Na/Sr O_{12} cuboctahedra, which increase in size and become more regular. A more geometric approach to describe the distortions of the perovskite structure is given by Goldschmidt's tolerance factor $t = (R_A + R_O)/[2^{1/2}(R_M + R_O)]$. A tolerance factor $t = 1.0$ favors an ideal cubic perovskite structure and values deviating from 1.0 tilted structures. The tilting scheme $a^-b^+a^-$ corresponding to the GdFeO_3 -type structure (space group $Pnma$) is frequently found when the A-cation is too small for the AO_{12} -cuboctahedra, $t < 1.0$, as this tilting maximizes A–O bonding interactions. For NaNbO_3 and SrNbO_3 the values for t are 0.965 and 0.967, respectively. It is therefore not surprising that both phases $\text{Na}_{0.7}\text{Sr}_{0.3}\text{NbO}_3$ and $\text{Sr}_{0.95}\text{NbO}_3$ (17) adopt GdFeO_3 -type structure. However, several modifications of NaNbO_3 exist

TABLE 7
Anisotropic Atomic Displacement Parameters (\AA^2) for $\text{Na}_{1-x}\text{Sr}_x\text{NbO}_3$, $x = 0.5$ and 0.6 (within the Parentheses) from Structure Refinements Based on the NPD Data

| Atom | $\beta_{11} = \beta_{22}$ | | β_{33} | | β_{12} | |
|-------|---------------------------|-------------|--------------|------------|--------------|--------------|
| Na/Sr | 0.0083(8) | (0.0078(7)) | 0.012(3) | (0.012(3)) | −0.0003(8) | (−0.0029(7)) |
| Nb | 0.0009(6) | (0.0013(6)) | 0.011(2) | (0.007(2)) | 0 | (0) |
| O1 | 0.014(1) | (0.012(1)) | 0.006(3) | (0.004(3)) | 0 | (0) |

Note. Anisotropic temperature factor = $\exp(-(\frac{1}{2}h^2\beta_{11} + k^2\beta_{22} + l^2\beta_{33} + 2hk\beta^{12} + 2hl\beta^{13} + 2kl\beta^{23}))$.

TABLE 8
Selected Interatomic Distances (Å) and Angles (deg) for Na_{1-x}Sr_xNbO₃, 0.3 ≤ x ≤ 0.7 Calculated with Coordinates from the Refinements Using the XRD Data

| x = | 0.3 | 0.4 | 0.5 | 0.6 | 0.7 |
|-------------|-----------|----------|----------|----------|----------|
| Na/Sr-4·O1 | 2.7905(1) | 2.800(1) | 2.809(1) | 2.818(1) | 2.829(1) |
| Na/Sr-4·O2 | 2.639(2) | 2.677(2) | 2.692(1) | 2.718(2) | 2.723(2) |
| Na/Sr-4·O2' | 2.966(2) | 2.942(2) | 2.943(1) | 2.930(3) | 2.933(2) |
| Nb-2·O1 | 1.9829(1) | 1.989(1) | 1.994(1) | 1.998(1) | 1.996(1) |
| Nb-4·O2 | 1.987(2) | 1.989(2) | 1.994(2) | 1.998(3) | 2.006(3) |
| Nb-O2-Nb | 166.6(1) | 169.2(1) | 169.8(1) | 171.4(2) | 171.5(2) |

and none of the crystallizes in the space group *Pnma*. On the other hand, the most well-known modification of Sr_xNbO₃ (0.7 ≤ x ≤ 0.95) is cubic (12). Similar *t*-values for NaNbO₃ and SrNbO₃, therefore, indicate that the changes in the structure, when replacing Na by Sr, probably is to a large extent due to the population of Nb–O π-bonding interactions favoring an Nb–O–Nb bond angle of 180°. A comparison between tetragonal single-tilt system *a*⁰*a*⁰*c*⁺ (*P4/mbm*) and the orthorhombic triple-tilt *a*⁻*b*⁺*a*⁻ (*Pnma*) found for one of the x = 0.6 samples reveals that only a minor change in tilt angle is needed for a transformation between the structures. It is, therefore, not surprising that the ED studies show an intergrowth of tetragonal and orthorhombic domains in the crystallites. It seems quite reasonable to assume that areas of the double-tilt system *a*⁰*b*⁻*c*⁺ with space group *Cmcm* exist because the screw axes in *P4/mbm* and *Pnma* were not always observed in the CBED patterns, but it has not been possible to finally ascertain it during this study. The structural variations indicated by the SAED/CBED study are most probably caused by small variations in the Na and Sr contents, combined with vacancies at these positions (it should be mentioned that Na is quite volatile at 1400°C).

The results from the structure refinements show that the compositional semiconductor–metallic transition observed

TABLE 9
Selected Interatomic Distances (Å) and Bond Angles (deg) for Na_{1-x}Sr_xNbO₃, x = 0.5 and 0.6 Calculated with Coordinates from the NPD Refinements

| x | 0.5 | 0.6 |
|---------------|-----------|-----------|
| Na1/Sr1-4·O1 | 2.8100(3) | 2.8189(3) |
| Na1/Sr1-4·O2 | 2.687(1) | 2.707(1) |
| Na1/Sr1-4·O2' | 2.949(1) | 2.944(1) |
| Nb-2·O1 | 1.9940(3) | 1.9993(3) |
| Nb-4·O2 | 1.996(2) | 2.000(2) |
| O1-Nb-O1 | 169.35(8) | 170.35(8) |

between Na_{1-x}Sr_xNbO₃, x = 0.5 and 0.6, are not caused by major structural changes. The metallic conductivity of Na_{1-x}Sr_xNbO₃, x ≥ 0.6, samples is simply an effect of a larger number of charge carriers in the conduction bands. Resistivity data for the metallic Na_{1-x}Sr_xNbO₃, x = 0.7, 0.8 and 0.9 samples show a linear dependence of the resistivity vs temperature: $\rho = \rho_0 + AT$. This indicates an electron–phonon scattering mechanism. For the metallic Na_{0.4}Sr_{0.6}NbO₃ $\rho(T)$ dependence is more complex and cannot be fitted by linear function.

As was indicated earlier for the x = 0.4 and 0.5 compositions, a maximum on the resistivity curves was observed at about T = 70 and 80 K, respectively. Such a temperature behavior of the resistivity is not rare. In the system La_{1-x}TiO₃, 0.0 ≤ x ≤ 0.33, a maximum of the resistivity (18) was observed for the composition La_{0.75}TiO₃ which is between the compositions La_{0.7}TiO₃ and La_{0.8}TiO₃, being insulating and metallic, respectively. The authors supposed that disorder-induced localization might play a role in the localization mechanism for La_{0.75}TiO₃. The complex temperature-dependent behavior of the electrical resistivity of the Na_{1-x}Sr_xNbO₃ samples with x = 0.4 and 0.5 might be also related to a fluctuation of the charge carrier concentrations in different crystallites caused by local variations in the Na/Sr ratio combined with vacancies at these positions.

ACKNOWLEDGMENTS

The authors thank the Royal Swedish Academy of Sciences, Mr. Håkan Rundlöf and Dr. Sten Eriksson at NFL, Studsvik, for the NPD data and the Swedish Research Council, A. Simon and the Max-Planck-Gesellschaft for the financial support.

REFERENCES

1. J. B. Goodenough, *Prog. Solid State Chem.* **5**, 145 (1971).
2. J.-E. Weber, C. Kegler, N. Büttgen, H.-A. Krug von Nidda, A. Loidl, and F. Lichtenberg, *Phys. Rev. B* **64**, 235 414 (2001).
3. T. Arima, Y. Tokura, and J. B. Torrance, *Phys. Rev. B: Condens. Matter* **48**, 17 006 (1993).
4. G. Amow, N. P. Raju, and J. E. Greedan, *J. Solid State Chem.* **155**, 177 (2000).
5. S. Y. Istomin, G. Svensson, H. Hannerz, and J. Köhler, *J. Solid State Chem.* **154**, 427 (2000).
6. S. Y. Istomin, G. Svensson, H. Hannerz, and J. Köhler, *Solid State Sci.* **4**, 191 (2002).
7. A. M. Glazer, *Acta Crystallogr. A* **31**, 756 (1975).
8. B. Ellis, J.-P. Doumerc, M. Pouchard, and P. Hagenmüller, *Mater. Res. Bull.* **19**, 1237 (1984).
9. B. Ellis, J.-P. Doumerc, P. Dordor, M. Pouchard, and P. Hagenmüller, *Solid State Commun.* **51**, 913 (1984).
10. S. Y. Istomin, G. Svensson, O. G. D'Yachenko, W. Holm, and E. V. Antipov, *J. Solid State Chem.* **141**, 514 (1998).
11. F. Izumi, *Rigaku J.* **6**, 10 (1989).

12. D. Ridgley and R. J. Ward, *J. Am. Chem. Soc.* **77**, 6132 (1955).
13. R. D. Shannon, *Acta Crystallogr. A* **32**, 751 (1976).
14. I. N. Flerov, M. V. Gorev, K. S. Aleksandrov, A. Tressaud, J. Grannec, and M. Couzi, *Mater. Sci. Eng.* **24**, 81 (1998).
15. C. N. W. Darlington and K. S. Knight, *Acta Crystallogr. B* **55**, 24 (1999).
16. M. Ahtee and C. N. W. Darlington, *Acta Crystallogr. B* **36**, 1007 (1980).
17. H. Hannerz, G. Svensson, S. Y. Istomin, and O. G. D'Yachenko, *J. Solid State Chem.* **147**, 421 (1999).
18. M. J. Maceachern, H. Dabkowska, J. D. Garrett, G. Amow, W. H. Gong, G. Liu, and J. E. Greedan, *Chem. Mater.* **6**, 2092 (1994).